Microfluidics and Nanofluidics (2022) 26: 72
https://doi.org/10.1007/s10404-022-02579-3

RESEARCH PAPER

A practical and cost-effective method to make permanently bonded acoustofluidic chips reconfigurable

Furkan Kuruoğlu[1]

Received: 22 June 2022 / Accepted: 17 August 2022 / Published online: 29 August 2022

Abstract
Acoustofluidic devices that save space and cost are promising for in-situ diagnosis and also the prognosis of many diseases including bacterial infections and cancer. Acoustofluidic devices owe their merit to the combined use of two functional materials, usually lithium niobate and polydimethylsiloxane. While the permanent bonding between lithium niobate-based surface acoustic wave chips and polydimethylsiloxane-based microchannel gives a wide range of functionality, it inevitably limits such devices to single-purpose use where versatility is absent. Here, a bond-detach procedure was demonstrated as a practical and cost-efficient method that enables design modification either in a lithium niobate chip or microchannel. Hence, by simply replacing either constituent, modified acoustofluidic devices targeted for different microbody types or sizes can be realized. The proposed approach to detach permanently bonded acoustofluidic devices via oxygen plasma treatment is based on immersing the devices in 0.1 M potassium hydroxide solution for two hours. It is clearly seen that the bond-detach procedure can be applied at least three times without any significant deterioration in either piezoelectric surface or microfluidic channel in terms of mechanical, optical and chemical properties. Moreover, no significant shift or attention was observed in the transmission spectra of interdigital transducers pairs after the application of the procedure three times. The proposed approach can help durability and reusability of acoustofluidic devices against factors such as clogging, and mechanical or chemical degradation.

1 Introduction

Microfluidics has been used to manipulate small amounts of fluids and micro/nanoparticles in microchannels for several decades. Applications and research on body-cells (Wu et al. 2021; Mirakhorli et al. 2022), bacteria (Fang et al. 2021; Geersens et al. 2022), drugs (Forigua et al. 2021; Zhao et al. 2021), microvesicles (Lin et al. 2021; Tamrin et al. 2021), etc., are of significant interest in microfluidics. Separating or patterning the particles in a microchannel still has numerous applications in microfluidics. Accordingly, the importance of contact-free control and manipulation methods that preserve cell viability in microfluidic applications is elevating, as most applications deal with biomaterials. Therefore, surface acoustic waves (SAWs) stand out as they enable harmless and non-contact manipulation of bio-associated particles, which can range in size from nanometers to micrometers.

The most common way to generate SAWs is creating time-harmonic mechanical displacement patterns on a piezoelectric surface by applying time-varying voltage in radio frequency (RF) frequencies with an electrode pair in the form of an interdigital transducer (IDT). Even though several other piezoelectric materials like lead zirconate titanate (PZT) (Salari et al. 2021; Liu et al. 2022), quartz (Wang et al. 2020) and ZnO (Wang et al. 2021) are also used for SAW generation, lithium niobate ($LiNbO_3$) is the most widespread substrate of choice because of its superior properties, such as high electromechanical coupling coefficient and SAW velocity (Devendran et al. 2020; Dai Nguyen et al. 2020; Afzal et al. 2021). Polydimethylsiloxane (PDMS) is the most prevalent material in microfluidics, especially acoustofluidics, because of its compatibility with biological samples, affordability and convenience in fabrication. High optical transmittance, flexibility and the possibility of permanent bonding to different surfaces are other advantages of PDMS.

Most acoustofluidic devices are used following permanent bonding of the PDMS-based microchannel and the $LiNbO_3$-based SAW chip. This confines the design and application of both piezoelectric chip and microchannel for single-use where a particular biomaterial type and/or size is

✉ Furkan Kuruoğlu
furkan.kuruoglu@istanbul.edu.tr

[1] Department of Physics, Faculty of Science, Istanbul University, Vezneciler, 34134 Istanbul, Turkey

Graphical abstract

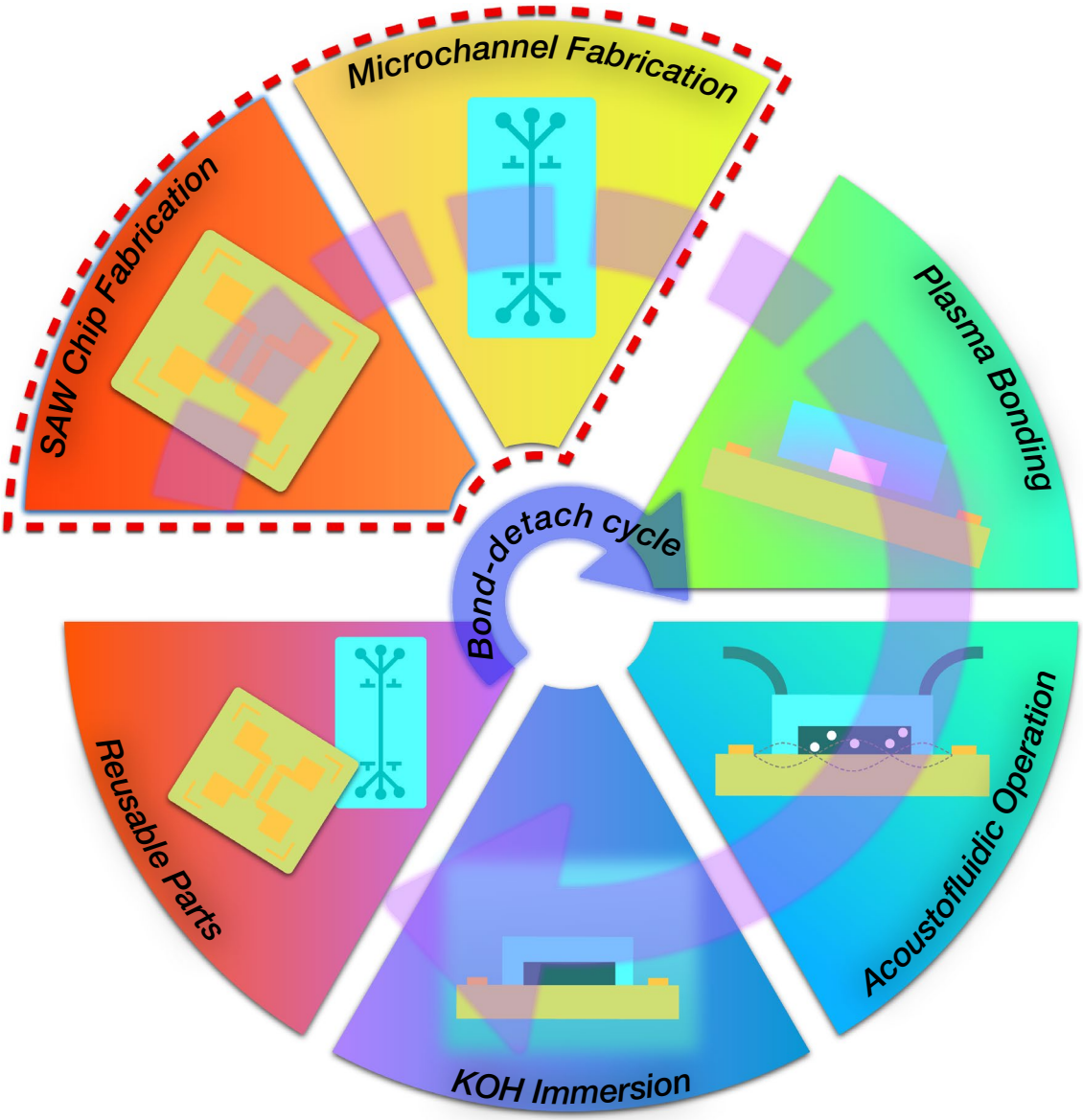

Keywords Acoustofluidic · Lithium niobate · PDMS · KOH · Bond-detach

considered (Zhao et al. 2020). For instance, if an acoustofluidic device is designed to separate a specific cell type from blood cells, it would be beneficial to redesign a microchannel for a different cell type with different width and an output channel distribution while keeping the SAW chip.

Multi-purpose use of acoustofluidic chips in a reconfigurable manner requires an appropriate method for numerous bond-detach cycles of permanently bonded SAW chips and PDMS microchannels without leaving residue on the piezoelectric surface, with the ability to strong rebonding while preserving surface integrity of PDMS microchannel, as well as mechanical, optical, electrical, chemical, etc. properties of the constituents. In addition, such a method should also be practical, achievable via common cleanroom chemicals and tools, repeatable and cost-effective.

In this work, a practical and cost-effective method that enables multiple uses of acoustofluidic devices in a reconfigurable manner, where not only the permanently bonded SAW chip but also the PDMS microchannel is preserved after several bond-detach cycles is demonstrated. The

method relies on simply immersing the acoustofluidic device in potassium hydroxide (KOH) for several hours, detaching the components and rebonding via oxygen plasma. After each bond-detach cycle, the RF transmission and optical characterization of the SAW chip, as well as surface morphology, hydrophobicity, Fourier-transform infrared (FTIR), and optical transmission analyses of PDMS microchannel are carried out. The bonding strength was also mechanically tested for each reusage cycle of the acoustofluidic chip. It is believed that the proposed bond-detach method expedites the advance of multi-purpose acoustofluidic chips with interchangeable SAW chips and PDMS microchannels.

2 Experimental

2.1 IDT fabrication

Figure 1a represents the schematic illustration of SAW chip. 300 µm thick double-side polished Y-128° $LiNbO_3$ was used as a substrate for the chip fabrication. $LiNbO_3$ substrate was then coated with AZ5214E (Microchemicals, Germany) photoresist with a thickness of ≈1.5 µm. The chirped IDT design was transferred to the substrate surface using a mask-aligner (MJB4-Suss, Germany) equipped with a 405 nm UV lamp. Ni was chosen for an adhesive layer due to its persistent nature to KOH (Williams et al. 2003). 10 nm Ni and 100 nm Au were sequentially evaporated and immersed in acetone for the lift-off process. The microscope image in Fig. 1b represents the patterned Chirped IDT on $LiNbO_3$.

2.2 PDMS fabrication and bonding

SU-8 2050 (Microhemicals, Germany) was used as a master mold on a Si wafer. Sylgard 184 PDMS kit (Dow-Corning) was used for microchannel fabrication. The base polymer and the curing agent were mixed at a 10:1 weight ratio, respectively. The degassed PDMS blend was poured in a sarcophagus mold including a 2-mm thick 3D printed spacer that adjusts the microchannel thickness and a PMMA cover ensures the perfectly parallel two surfaces as described (Cottet et al. 2017). $LiNbO_3$ and PDMS surfaces were activated by oxygen plasma (Diener Zepto, Germany) for irreversible bonding. 20 W plasma power was used to support the plasma and 1 mbar chamber pressure was fixed for 120 s (Bhattacharya et al. 2005). Precise alignment was carried out between the $LiNbO_3$ chip and PDMS microchannel using the marks as shown in Fig. 1c (Cottet et al. 2017). The aligned device was annealed at 85 °C for 5 min to strengthen the bonding between $LiNbO_3$ and PDMS and the alignment and bonding were checked visually by an optical microscope Fig. 1d.

2.3 Electrical characterization of IDTs

Radio frequency (RF) reflection (S_{11}) spectra of IDTs were measured by a 6 GHz vector network analyzer (PicoVNA-106, UK). Calibration was carried out from 15 to 40 MHz with a frequency step of 500 Hz.

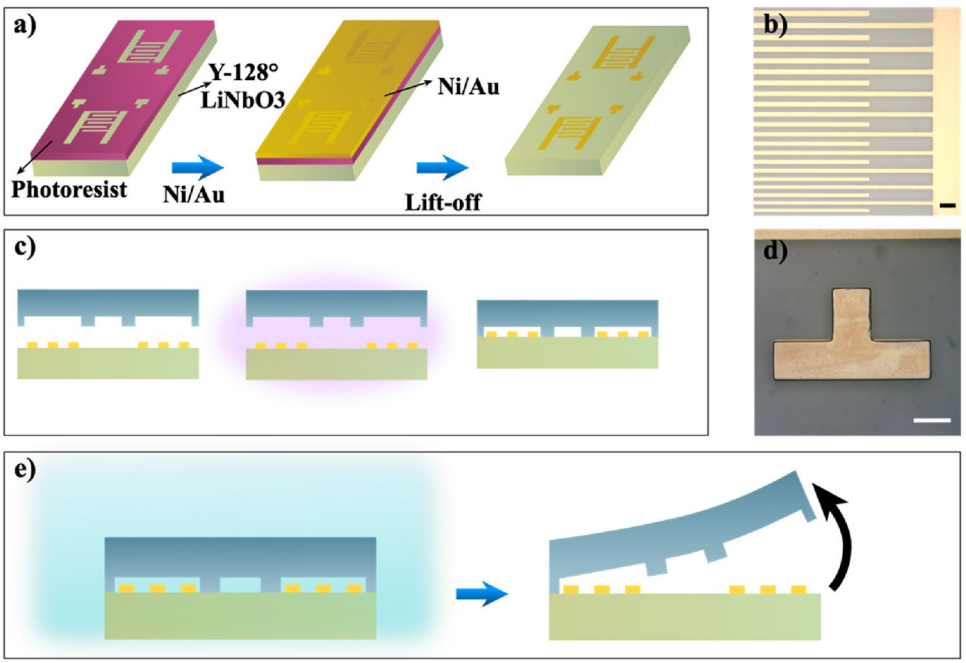

Fig. 1 **a** Schematic description of standard photolithography process of the oppositely facing IDT pairs, **b** optical microscope image of the chirped IDT fingers, **c** plasma bonding illustration of $LiNbO_3$ chip and PDMS microchannel in O_2 environment, **d** image of the perfectly aligned marker on $LiNbO_3$ and PDMS and **e** illustration of detaching process by immersing the sample in KOH solution and the prelease of the PDMS microfluidic channel (scale bar is 150 µm)

2.4 Optical transmission measurement

The optical transmission was examined for LiNbO3 and PDMS samples in the range from 200 to 1000 nm to observe the transmittance change with bond-detach cycles. A fiber-coupled illumination source equipped with a deuterium and halogen lamp (Ocean Optics, UK) was used. Si CCD array spectrometer (Ocean Optics, UK) was used to collect the spectra and OceanView software was used for controlling the spectrometer and transforming the measured spectra to transmission.

2.5 Surface characterization

PDMS surfaces were investigated by an Atomic Force Microscopy (AFM) (XE-100 Park System, Korea) to determine the surface properties like roughness and waviness, in non-contact mode with a Si cantilever. 25 μm × 25 μm scan area was determined which is located 100 μm away from the alignment mark. Post-leveling and statistical analysis were carried out using open-source Gwyddion software (Nečas and Klapetek 2012). The hydrophilicity of the $LiNbO_3$ and PDMS surfaces was utilized with the contact angle measurements between the water droplet and the surfaces. 0.5 μL water droplets were dripped on the surfaces using an adjustable micropipette which was mounted on an *X–Y–Z* micropositioner stage and images were captured with a USB-controlled microscope camera. The contact angle values were measured on ImageJ (Schindelin et al. 2012). The energy-dispersive X-ray spectroscopy (EDS) and scanning electron microscopy (SEM) images were obtained using Versa 3D Dual Beam (FEI, USA) equipped with Octane Super SD detector (Ametek, USA). 5 kV acceleration voltage was used to achieve surface sensitivity and the EDS detector has 128 eV resolution.

2.6 Detach process

PDMS microchannel and $LiNbO_3$ chip were durably bonded as described. After 90 min later from the bonding process, bonded samples were immersed in 0.1 M KOH (Merck, Germany) solution for 2 h. Thereafter, the detached PDMS microchannel and $LiNbO_3$ chip were rinsed with DI water and dried with nitrogen blow.

2.7 Fourier-transform infrared spectrometry measurement

The changes in the chemical bonding were analyzed through FTIR Spectrometry measurements. The FTIR data were collected on Nicolet 10 iS (Thermo Fisher) FTIR spectrometer at a range of 4000–500 cm^{-1}. Transmittance-wavenumber spectra were recorded with 2 cm^{-1} resolution for all measurements.

2.8 Bonding strength test

A leakage test was performed using New-Era 300 programmable syringe pump tubed with 1.8 mm diameter PTFE tubing. The flow rate was set as 10 μL/min and increased to 500 μL/min with 50 μL/min steps. 5 min of dwell time was applied for every flow rate step.

Tensile strength measurements were recorded on Instron 8872 testing system. 0.5 mm/min extension rate was used for the measurement of all devices.

3 Results and discussion

In Fig. 2, RF reflection spectrum (S_{11}) is plotted as a function of frequency after each KOH treatment. Corresponding to the IDT finger width ranging from 30 to 50 μm with a thickness change of 5 μm between subsequent finger pairs, where each IDT has $N = 11$ finger pairs, the center peak was observed at ≈ 25 MHz as expected for the reference sample. Electrical measurements were repeated after each bonding and detaching process, and no shift was observed in the S_{11} spectrum. In addition to this, no significant change in peak intensity was observed, which is also related to SAW power.

It should be noted that the preserving electrical characteristics of the SAW chip after KOH immersion during the detach process is strongly dependent on IDT contact material. As an adhesive layer, a thin Ni is not affected by KOH and thus, stable electrical characteristics could be achieved.

Figure 3a–d shows the surface morphologies of the reference and bond-detached PDMS surfaces. Native PDMS has 1.58 nm RMS surface roughness (S_q) and distributed pinholes on the whole ROI surface (Pinto et al. 2010; Thurgood et al. 2019; Hoppe et al. 2022), while the surface roughness increases and the pin-hole formation disappears by increasing the number of bond-detach processes. Dinh et al. (2015) reported a similar increment on the PDMS surface roughness hereafter a mechanical peeling procedure due to the transferred thin PDMS layer.

In comparison, the direct peeling of PDMS right after the KOH immersion procedure is also characterized by AFM and EDS measurements, as seen in Figs. S1 and S2. Even if the remnant PDMS layer can be dissolved by KOH without any residual leftovers, surface roughness is determined to be much higher than the procedure reported in this work (Dinh et al. 2015). The cross-sectional height profiles of the surfaces were plotted in Fig. 3e to visualize the change more conspicuously. It is clearly seen that the surface profile changes from rough to wavy with the number of treatment cycles.

The optical transparency of $LiNbO_3$ and PDMS over a wide spectral range is one of the reasons for their use in lab-on-chip applications, providing ease of observation as well as operation of chips. Herewith, transmittance spectra were measured in the UV and visible regions for the $LiNbO_3$ and PDMS parts of the chip following each bond-KOH immersion cycle to identify the dependencies of the optical transparency to the detach treatment. As can be seen from Fig. 4, both $LiNbO_3$ chips and PDMS have 85% and 90% transparency, respectively, in the visible region, even after the third KOH-based detach treatment. The bond-detach cycles have shown no negative influence on the optical transparency of $LiNbO_3$ chips at the examined spectral range.

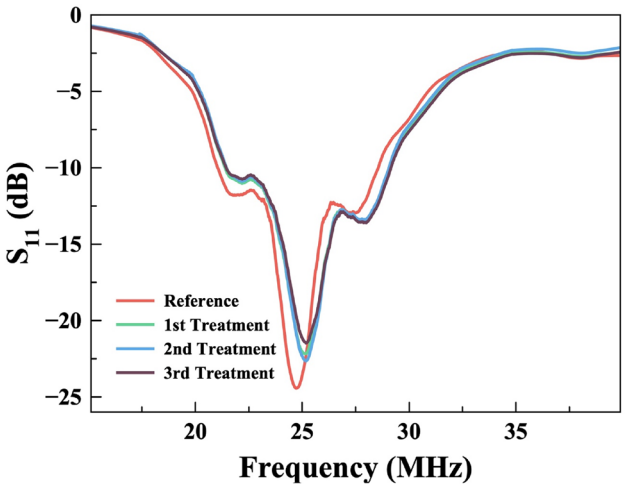

Fig. 2 RF transmission spectra of bare and PDMS bond-detached $LiNbO_3$ chips. As fabricated $LiNbO_3$ chip was used as the reference sample

There was seen a characteristic valley in transmittance spectra of the PDMS around 275 nm, which was previously reported by many researchers (Xu et al. 2009; Ren and Liu 2019; Zhu et al. 2019). This valley in transmittance tails off steadily by the bond-detach treatment. This behavior may be attributed to the diminished effect of the pin-hole formation, which causes Rayleigh scattering on the PDMS surface in the mentioned spectral region. Scattered light from the surface reduces the transmittance. After the KOH-based detach treatment, since a wavy surface is formed, the scattering effect reduces.

The transition from hydrophobic to hydrophilic characteristics via plasma activation is a well-known native PDMS and $LiNbO_3$ feature (Maji et al. 2012). Figure 5a, b shows the contact angle micrographs of $LiNbO_3$ and PDMS as a function of bond-detach cycle number. Even though different contact angles were reported for the bare $LiNbO_3$ (Xu et al. 2018; Yang et al. 2021), whole contact angles were shown in Fig. 5a keep in the range of the literature. This trend confirms the detach process recurs the $LiNbO_3$ surface to its initial form.

The contact angle of native PDMS was measured as $102° \pm 2°$ which has a good agreement with the literature (Li and Liao 2016; Hassanpour-Tamrin et al. 2021; Kaczorowski et al. 2021). With the bond-detach cycle, a slight increment was also observed at the contact angle as seen in Fig. 5b, c. The increased roughness after the same sequence of processes causes a higher contact angle than the initial surface (Khorasani et al. 2005). The measured contact angles of both $LiNbO_3$ and PDMS indicate the increased surface energy wanted for the bonding process is reverted to its original value.

FTIR Spectra were collected from the PDMS surfaces to enlighten the behavior of the chemical bonds related to $LiNbO_3$-PDMS bonding. In the presence of the full-range

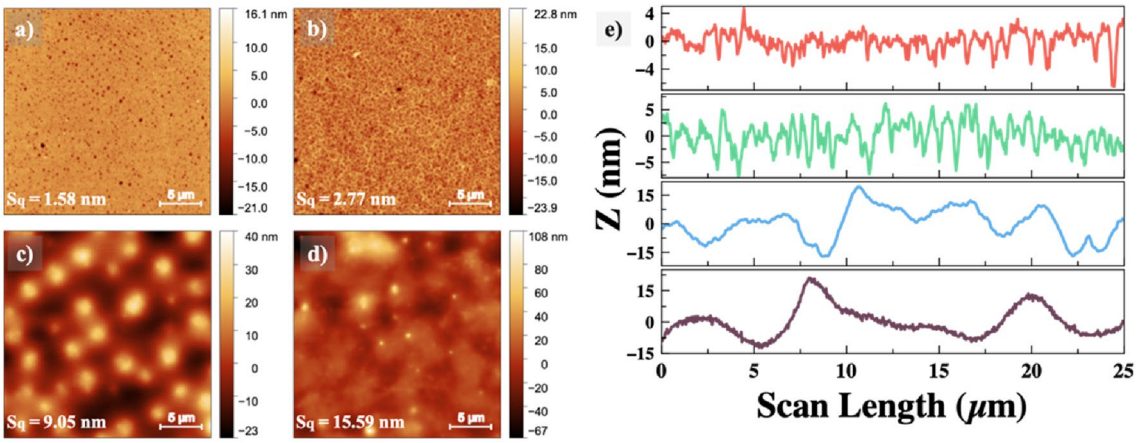

Fig. 3 AFM images of the **a** native PDMS surface as reference and treated PDMS surfaces after **b** 1st, **c** 2nd and **d** 3rd cycle of bond-detach process. **e** Cross-sectional surface profiles of reference and after 1st, 2nd and 3rd treatment plotted as red, green, blue and dark violet, respectively

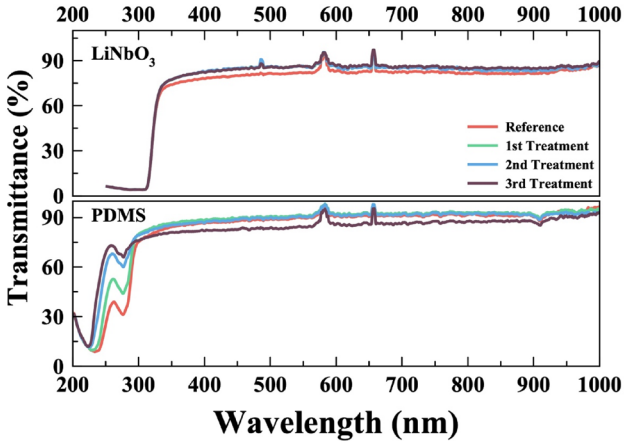

Fig. 4 Optical transmittance spectra in the UV–Vis region for $LiNbO_3$ and PDMS samples

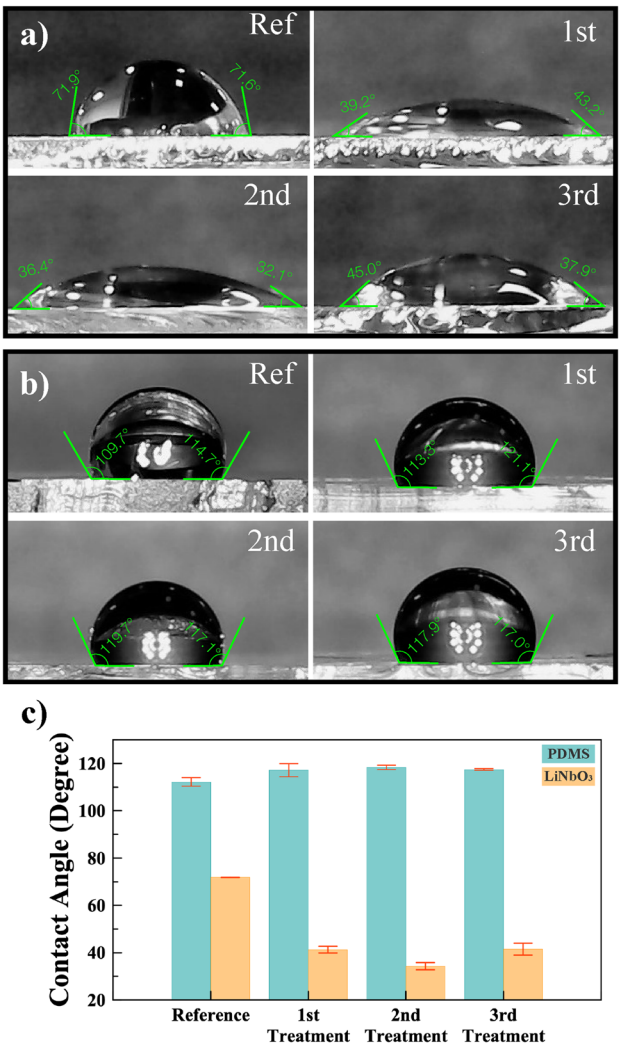

Fig. 5 Water contact angle images of **a** $LiNbO_3$ and **b** PDMS surfaces. **c** The contact angles of the $LiNbO_3$ and PDMS versus the number of bond-detach treatments

spectra given in Fig. 6, all samples show the characteristic PDMS transmission peaks. The peak coincides in the 3050–3700 cm^{-1} region is attributed to –OH functional groups (Maji et al. 2012). The zoomed plot of the mentioned region in Fig. 6 presents peak variation with the treatment. The reference sample has no peak related to the –OH groups while the O_2 plasma-treated has as expected. Due to the increasing peak intensity of the bond-detach treatment can be considered as KOH immersion has no detractive effect on –OH groups. The serial O_2 plasma treatment leads to an increment in the peak intensity. Another zoomed inset spectra in the region of 900–1100 cm^{-1} is associated with the Si–O–Si signal (Lamberti et al. 2015; Ren and Liu 2019). As the KOH targets the siloxane groups (Szilasi and Cserháti 2018) of silica formed by the plasma treatment in the depth of a few tens of nanometers on the PDMS surface (Ohishi et al. 2016), related peak intensities decrease consistently after the detach process.

Bonding strength tests were carried out to ensure the effective bonding formed between the detached $LiNbO_3$ and PDMS samples. At first, leakage tests were performed on the re-bonded devices after the detachment. The fluid rate was set to a maximum of 500 µL/min and no leakage was observed at neither reference nor the re-bonded devices. The bond of all devices withstands the microchannel pressure of ~ 463 kPa at the driven maximum flow rate which is derived using the Hagen-Poiseuille equation. The bonding strength between the $LiNbO_3$ and PDMS was also determined by the tensile test. Measured tensile stress and load-time graphs are presented in Fig. 7a, b respectively.

As can be seen from the Fig. 7a, no significant bonding strength-loss was observed for the whole devices. Achieving smaller surface roughness may lead to better adhesion between the $LiNbO_3$ and PDMS which yields that satisfactory tensile strength even after the third bond-detach cycle. In addition to this, more brittle-like bonding behavior was observed as the bond-detach cycles increase as seen in Fig. 7b. From the slope of the load-time plot, elastic modules of the bonds were calculated and consistent increment was observed. This behavior may be the effect of the increasing time exposed to temperature requires for repeating bond-detach cycles. Figure 7c verifies the effective bonding formation on the whole device surface between $LiNbO_3$ and PDMS except for microchannel regions for all devices.

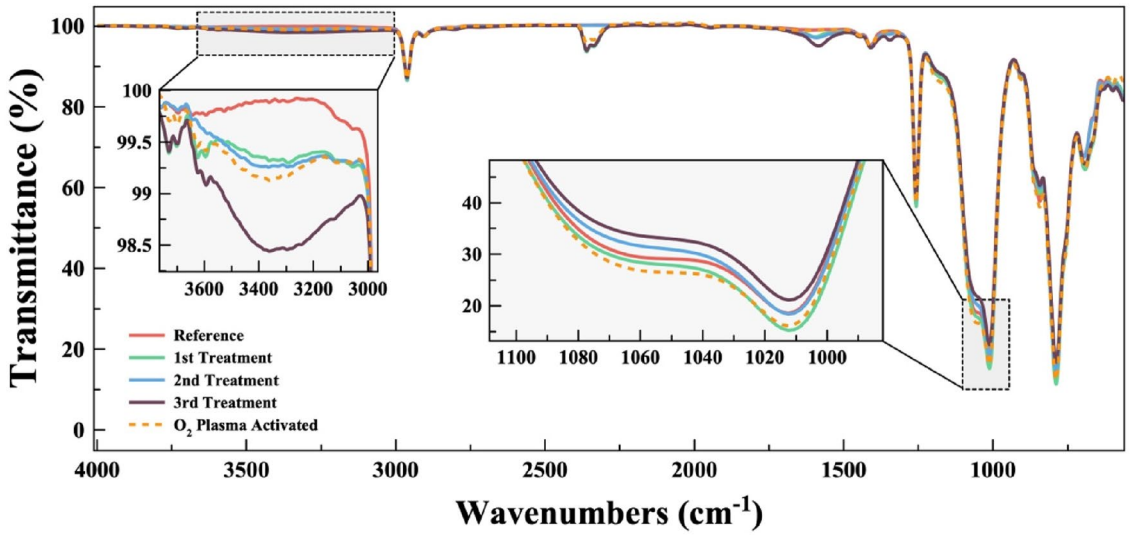

Fig. 6 FTIR spectra of the PDMS samples. The insets represent the zoomed-in view of the highlighted peak regions

4 Conclusion

In this study, a simple and efficient bond-detach procedure was reported and its effects on the $LiNbO_3$ chip and PDMS microchannel were investigated using RF spectra, AFM, UV–Vis transmission, wettability, FTIR and bonding strength measurements as a function of the bond-detach cycles. It was concluded that the reported procedure has no significant influence on the electrical, optical and wettability properties of the $LiNbO_3$ chip. In terms of PDMS, it was ensured that the surface roughness increased and pinhole formation on the native PDMS surface disappeared hence the optical transmission shows an increment in the UV region. The contact angle and FTIR measurement finding indicate the reported process recovers the bonded PDMS surface to its initial. Also, FTIR peak behaviors related to the –OH and Si–O groups reveals the mechanism that corresponds to the detachment with the KOH immersion. Bonding strength and microchannel leakage tests reveal that no weakening occurred after the bond-detach cycles. Both examinations showed that the microfluidic device can withstand up to 463 kPa pressure even after the 3rd bond-detach cycle.

Taking into account all of these findings from the systematic measurements, the reported bond-detach procedure uses the O_2 plasma activation and room temperature KOH immersion makes the chip and PDMS microchannel repeatedly usable by bond-detach cycles and also may pave the way for the multi-purpose single-chip acoustofluidic lab-on-a-chip applications. Thus, the proposed method will allow the use of more cost-effective microfluidic systems by reducing the need for new components constantly, and as a result, it is expected that it will contribute positively to the prevalence of microfluidic devices.

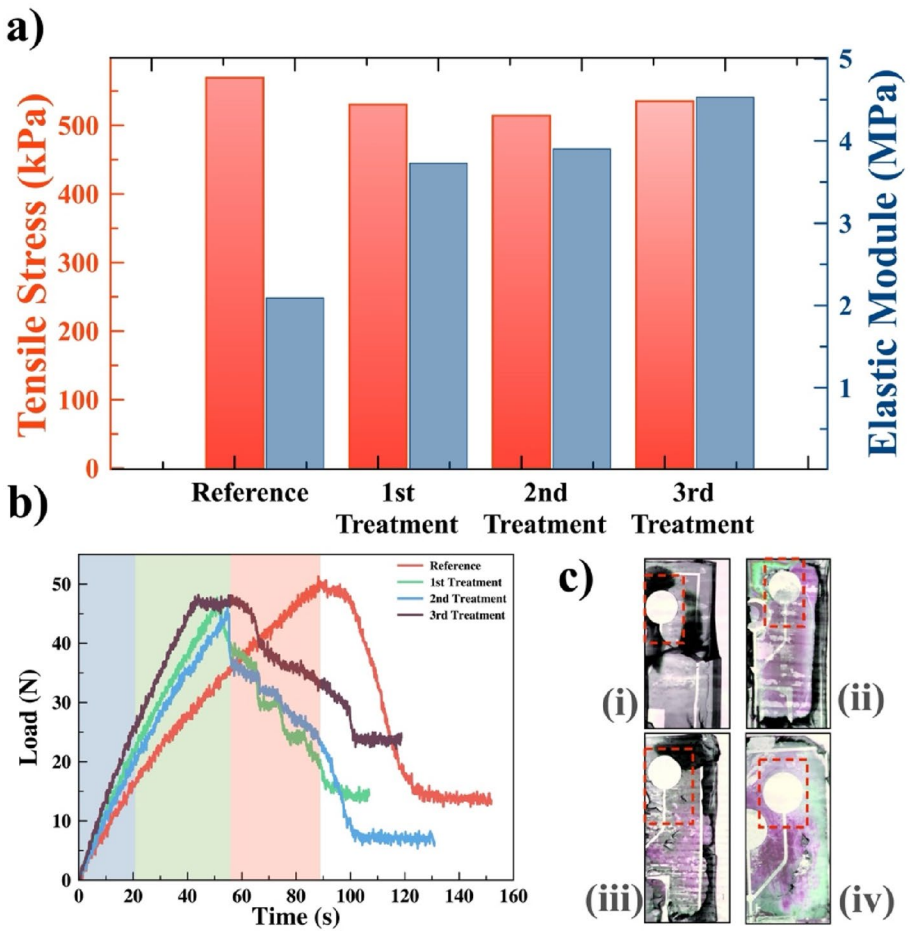

Fig. 7 **a** Tensile strength and the calculated elastic module of the bonded devices, **b** load versus time plot of the tested devices. The highlighted regions indicate the changing slope of the curves. **c** The images remanent on the surface after the bonding test. The red dashed regions indicate the efficient bond between the $LiNbO_3$ and PDMS. (i) represents the reference sample while (ii), (iii), (iv) represent the 1st, 2nd and 3rd time treated samples, respectively

Supplementary Information The online version contains supplementary material available at https://doi.org/10.1007/s10404-022-02579-3.

Acknowledgements I appreciate Ayse Aktas, Prof. Dr. Ahmet Cicek and Prof. Dr. Ayse Erol for their valuable support.

Funding The study is funded by The Scientific and Technological Research Council of Turkey (TUBITAK) (Project no: 120F337) and Istanbul University Scientific Research Projects Coordination under the Grant no. FBG-2021-37896.

Declarations

Conflict of interest The author has no relevant financial or non-financial interests to disclose.

References

Afzal M, Park J, Jeon JS et al (2021) Acoustofluidic separation of proteins using aptamer-functionalized microparticles. Anal Chem 93:8309–8317. https://doi.org/10.1021/acs.analchem.1c01198

Bhattacharya S, Datta A, Berg JM, Gangopadhyay S (2005) Studies on surface wettability of poly(dimethyl) siloxane (PDMS) and glass under oxygen-plasma treatment and correlation with bond strength. J Microelectromech S 14:590–597. https://doi.org/10.1109/jmems.2005.844746

Cottet J, Vaillier C, Buret F et al (2017) A reproducible method for µm precision alignment of PDMS microchannels with on-chip electrodes using a mask aligner. Biomicrofluidics 11:064111. https://doi.org/10.1063/1.5001145

Dai Nguyen T, Qing Fu Y, Tran V–T, Gautam A, Pudasaini S, Du H (2020) Acoustofluidic closed-loop control of microparticles and cells using standing surface acoustic waves. Sens Actuators B Chem 318:128143. https://doi.org/10.1016/j.snb.2020.128143

Devendran C, Choi K, Han J et al (2020) Diffraction-based acoustic manipulation in microchannels enables continuous particle and bacteria focusing. Lab Chip 20:2674–2688. https://doi.org/10.1039/d0lc00397b

Dinh THN, Cao HH, Hamdi FS et al (2015) Development of reversible bonding for microfluidic applications. Microfluid Nanofluidics 19:751–756. https://doi.org/10.1007/s10404-015-1599-8

Fang Y-L, Wang C-H, Chen Y-S et al (2021) An integrated microfluidic system for early detection of sepsis-inducing bacteria. Lab Chip 21:113–121

Forigua A, Kirsch RL, Willerth SM, Elvira KS (2021) Recent advances in the design of microfluidic technologies for the manufacture of drug releasing particles. J Control Release 333:258–268

Geersens É, Vuilleumier S, Ryckelynck M (2022) Growth-associated droplet shrinkage for bacterial quantification, growth monitoring, and separation by ultrahigh-throughput microfluidics. ACS omega

Hassanpour-Tamrin S, Sanati-Nezhad A, Sen A (2021) A simple and low-cost approach for irreversible bonding of polymethylmethacrylate and polydimethylsiloxane at room temperature for high-pressure hybrid microfluidics. Sci Rep UK 11:4821. https://doi.org/10.1038/s41598-021-83011-8

Hoppe C, Mitschker F, Mai L et al (2022) Influence of surface activation on the microporosity of PE-CVD and PE-ALD SiOx thin films on PDMS. Plasma Process Polym 19:2100174. https://doi.org/10.1002/ppap.202100174

Kaczorowski W, Świątek H, Łuczak K et al (2021) Impact of plasma pre-treatment on the tribological properties of DLC coatings on PDMS substrates. Materials 14:433. https://doi.org/10.3390/ma14020433

Khorasani MT, Mirzadeh H, Kermani Z (2005) Wettability of porous polydimethylsiloxane surface: morphology study. Appl Surf Sci 242:339–345. https://doi.org/10.1016/j.apsusc.2004.08.035

Lamberti A, Virga A, Rivolo P et al (2015) Easy tuning of surface and optical properties of PDMS decorated by Ag nanoparticles. J Phys Chem B 119:8194–8200. https://doi.org/10.1021/acs.jpcb.5b02581

Li C-Y, Liao Y-C (2016) Adhesive stretchable printed conductive thin film patterns on PDMS surface with an atmospheric plasma treatment. ACS Appl Mater Inter 8:11868–11874. https://doi.org/10.1021/acsami.6b02844

Lin B, Lei Y, Wang J et al (2021) Microfluidic-based exosome analysis for liquid biopsy. Small Methods 5:2001131

Liu P, Tian Z, Yang K et al (2022) Acoustofluidic black holes for multifunctional in-droplet particle manipulation. Sci Adv 8:eabm2592. https://doi.org/10.1126/sciadv.abm2592

Maji D, Lahiri SK, Das S (2012) Study of hydrophilicity and stability of chemically modified PDMS surface using piranha and KOH solution. Surf Interface Anal 44:62–69. https://doi.org/10.1002/sia.3770

Mirakhorli F, Mohseni SS, Bazaz SR, et al (2022) Microfluidic platforms for cell sorting. Sustain Sep Eng Mater Tech Process Dev 653–695

Nečas D, Klapetek P (2012) Gwyddion: an open-source software for SPM data analysis. Cent Eur J Phys 10:181–188. https://doi.org/10.2478/s11534-011-0096-2

Ohishi T, Noda H, Matsui TS et al (2016) Tensile strength of oxygen plasma-created surface layer of PDMS. J Micromech Microeng 27:015015. https://doi.org/10.1088/0960-1317/27/1/015015

Pinto S, Alves P, Matos CM et al (2010) Poly(dimethyl siloxane) surface modification by low pressure plasma to improve its characteristics towards biomedical applications. Colloids Surf B Biointerfaces 81:20–26. https://doi.org/10.1016/j.colsurfb.2010.06.014

Ren L, Liu J (2019) Synthesis and gas transport properties of polyamide membranes containing PDMS groups. RSC Adv 9:9737–9744. https://doi.org/10.1039/c8ra10550b

Salari A, Appak-Baskoy S, Coe IR et al (2021) Dosage-controlled intracellular delivery mediated by acoustofluidics for lab on a chip applications. Lab Chip 21:1788–1797

Schindelin J, Arganda-Carreras I, Frise E et al (2012) Fiji: an open-source platform for biological-image analysis. Nat Methods 9:676. https://doi.org/10.1038/nmeth.2019

Szilasi SZ, Cserháti C (2018) Selective etching of PDMS: etching technique for application as a positive tone resist. Appl Surf Sci 457:662–669. https://doi.org/10.1016/j.apsusc.2018.06.280

Tamrin SH, Nezhad AS, Sen A (2021) Label-free isolation of exosomes using microfluidic technologies. ACS Nano 15:17047–17079

Thurgood P, Baratchi S, Arash A et al (2019) Asynchronous generation of oil droplets using a microfluidic flow focusing system. Sci Rep UK 9:10600. https://doi.org/10.1038/s41598-019-47078-8

Wang J, Guo Y, Li D et al (2020) Bacterial cellulose coated ST-cut quartz surface acoustic wave humidity sensor with high sensitivity, fast response and recovery. Smart Mater Struct 29:045037

Wang Y, Zhang Q, Tao R et al (2021) Flexible/bendable acoustofluidics based on thin-film surface acoustic waves on thin aluminum sheets. ACS Appl Mater Interfaces 13:16978–16986

Williams KR, Gupta K, Wasilik M (2003) Etch rates for micromachining processing—Part II. J Microelectromech Syst 12:761–778

Wu Y, Chattaraj R, Ren Y et al (2021) Label-free multitarget separation of particles and cells under flow using acoustic, electrophoretic, and hydrodynamic forces. Anal Chem 93:7635–7646. https://doi.org/10.1021/acs.analchem.1c00312

Xu H, Gomez-Casado A, Liu Z et al (2009) Porous multilayer-coated PDMS stamps for protein printing. Langmuir 25:13972–13977. https://doi.org/10.1021/la901797n

Xu J, Wang C, Tian Y et al (2018) Glass-on-$LiNbO_3$ heterostructure formed via a two-step plasma activated low-temperature direct bonding method. Appl Surf Sci 459:621–629. https://doi.org/10.1016/j.apsusc.2018.08.031

Yang X, Geng W, Bi K et al (2021) The wafer-level integration of single-crystal $LiNbO_3$ on silicon via polyimide material. Micromach Basel 12:70. https://doi.org/10.3390/mi12010070

Zhao S, Wu M, Yang S et al (2020) A disposable acoustofluidic chip for nano/microparticle separation using unidirectional acoustic transducers. Lab Chip 20:1298–1308. https://doi.org/10.1039/d0lc00106f

Zhao Z, Wang Z, Li G et al (2021) Injectable microfluidic hydrogel microspheres for cell and drug delivery. Adv Funct Mater 31:2103339

Zhu J, Nakakubo K, Mikami Y et al (2019) Investigation and modeling of UV band-pass-filtering white compound materials for potting or embedding in micro-optical applications. Opt Mater Express 9:1002. https://doi.org/10.1364/ome.9.001002